Front. Phys., 2014, 9(6): 768–773
DOI 10.1007/s11467-013-0375-z

RESEARCH ARTICLE

Electric and thermo spin transfer torques in Fe/Vacuum/Fe tunnel junction

Xing-Tao Jia[1,2], **Ke Xia**[1,†]

[1] *Department of Physics, Beijing Normal University, Beijing 100875, China*
[2] *Department of Physics and Chemistry, Henan Polytechnic University, Jiaozuo 454000, China*
Corresponding author. E-mail: †*kexia@bnu.edu.cn*

Received July 3, 2013; accepted August 6, 2013

We present first-principle calculations of electric and thermo spin transfer torques (STT) in Fe/Vacuum(Vac)/Fe magnetic tunnel junctions (MTJs). Our quantitative studies demonstrate rich bias dependence of STT and tunnel magneto resistance (TMR) behaviors with respect to the interface roughness. Thermoelectric effects in Fe/Vac/Fe MTJs is remarkable. We observe larger ZT of 6.2 in 8 ML clean Vacuum barrier, where the heavily restrained thermal conductance should be responsible for. Thermo-STT in Fe/Vac/Fe MTJs show same order as that in Fe/MgO/Fe MTJs with similar barrier thickness.

Keywords spin transfer torque, Fe/Vacuum/Fe tunnel junction, thermoelectric effect

PACS numbers 72.25.Ba, 85.75.-d, 72.10.Bg

Frontiers of Physics

1 Introduction

Extensive studies have made the magnetic tunnel junctions (MTJs), especially MgO-based one, great progress [1–9]. However, the comprehensive understanding of the tunnelling effect in the MTJs is still insufficient due to the complication of the metal-insulator interface. The most useful signals to understand the tunnelling effect in MTJs would be tunnel magneto resistance (TMR) and Spin-transfer torques (STT) [10, 11]. The STT provides more information of the spin transport through MTJ comparing with TMR. For example, when the applied bias is small, STT could be used to assess the sign of current spin polarization in the parallel configuration (PC).

The STT can be estimated by model calculation with lots of parameters [12–16], and parameter-free calculations using realistic electronic structure by wave-functional-matching method [17, 18], and multiple scattering Green's function approach [19]. When the multiple scattering within barrier is negligible, the in-plane STT ($T_{//}$) can be obtained by simply calculating the difference of spin-current between PC and anti-parallel configuration (APC) [12]:

$$T_{//}(\theta) = \frac{I_z^{(s)}(\pi) - I_z^{(s)}(0)}{2} \sin\theta \qquad (1)$$

where, $I_z^{(s)}(\theta) = \frac{\hbar}{2e}(I^{\uparrow} - I^{\downarrow})$ is the spin-current across the barrier with certain magnetization relative angle θ. $I^{\uparrow(\downarrow)} = \frac{1}{e}\int \mathrm{d}E[f_L(\epsilon) - f_R(\epsilon)] \cdot G^{\uparrow(\downarrow)}(\epsilon)$, is spin dependent electric current induced by applied electric bias $V_b = (\mu_L - \mu_R)/e$ or temperature gradient $\Delta T = T_L - T_R$, $G^{\uparrow(\downarrow)}(E)$ is energy-dependent conductance and $f_{L/R}(\epsilon) = [\mathrm{e}^{(\epsilon-\mu_{L/R})/(k_\mathrm{B}T_{L/R})} + 1]^{-1}$ is Fermi–Dirac distribution with given local chemical potentials $\mu_{L/R}$ and temperatures $T_{L/R}$. We define the bias torkance as $\tau_V = T_{\Delta V}/V_b$ and the thermo-torkance as $\tau_T = T_{\Delta T}/\Delta T$.The temperature gradient can induce remarkable STT as demonstrated by the recently theoretical and experimental studies [6, 20–25].

In the tunnel junctions such as Fe/GaAs/Fe and Fe/Vac/Fe, minority-spin channel dominates the transport process due to the resonant channels between metal-insulator interfaces [26–30]. We expect larger thermoelectric (spin) effects due to the strong energy dependence of resonant channel. Vacuum is a good heat insulator, which makes thermoelectric effects more pronounced. The well characterized interfaces in Fe/Vac/Fe MTJs also will be very useful for the understanding the tunnelling processor. In this paper, we present a parameter-free calculation on the STT in Fe/Vac/Fe MTJs as shown in Fig. 1. Our calculations indicate rich bias dependence of STT in Fe/Vac/Fe with respect to the interface roughness, and large thermoelectric effects

in Fe/Vac/Fe. In Section 2, we briefly introduce our modeling of the Fe/Vac/Fe MTJs and some essential details of our calculation. In Section 3, we discuss the electric bias induced STT in MTJs. In Section 4, we provide the results for the thermo-STT in MTJs. And finally, we summarize our results.

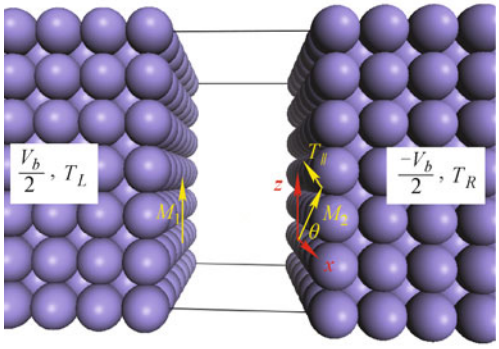

Fig. 1 Schematic Fe/Vac/Fe(001) MTJs with ideal interfaces. We consider both a temperature difference $\Delta T = T^L - T^R$ and voltage difference V_b between the ferromagnetic reservoirs. The magnetization $\boldsymbol{M}_1$ of the left lead is fixed along the z-axis, while the magnetization $\boldsymbol{M}_2$ of the right lead is rotated by an angle θ in the xz plane relative to $\boldsymbol{M}_1$.

2 Calculation methods

We consider a two-probe device consisting of a Vacuum barrier and two semi-infinite ferromagnetic leads with different magnetization directions as show in Fig. 1. The scattering region includes several buffer layers of lead atoms and several vacuum layers. We consider transport in the (001) growth direction keeping atoms at the surfaces unrelaxed in their bulk bcc position. An electric voltage V_b and a temperature gradient ΔT are applied at the leads to drive the current flow. We assume the imperfect only exist at the iron surfaces, the surface roughness is present in one atomic layer on both left or right Fe/Vac interfaces with x and $1-x$ Fe atoms to keep the average distance between the two interface is integral monolayer (ML) [30]. Here, we give a quantitative theoretic analysis of spin transport of the Fe/Vac/Fe MTJs based on density functional theory (DFT) calculation with the Keldysh nonequilibrium Green's function (NEGF) framework. The surface roughness or impurities scattering were deal at the single particle retarded Green's function level by coherent potential approximation (CPA) and at the NEGF level by evaluating a nonequilibrium vertex correction (NVC) term during the electronic structure and transport calculation [31].

Basically $T_{//}$ is calculated by Eq. (1). Moreover, as comparison and checking, we also calculated the STT directly by a tight-binding linear muffin-tin-orbital (TB-LMTO) wave-function-matching (WFM) calculation [17] based on DFT in the local density approximation (LDA) [32] with exchange-correlation potential parameterized by Vosko, Wilk, and Nusair [33]. For the STT calculation with scattering wave functions, we use 400×400 k mesh in the full two-dimensional Brillouin zone (BZ) to ensure excellent numerical convergence. The other details of the electronic structure and transport calculation can be found elsewhere [5, 27].

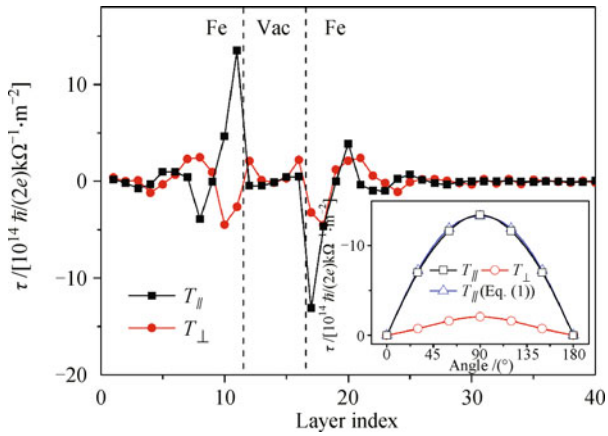

Fig. 2 Layer-resolved STT of 5ML vacuum barrier ideal junction with relative magnetization angle $\theta = \pi/2$ near zero bias. The lower insert is the angular dependence of total STT of the right side calculated by the scattering wave functions and Eq. (1).

To check the validity of Eq. (1), we calculated STT of Fe/Vac(5ML)/Fe with ideal interface under equilibrium state with scattering wave functions [17] as shown in Fig. 2. Therein, the magnetization angle θ between the left fixed and right free Fe leads sets to 90°. Obviously, both the $T_{//}$ and $T_\perp$ oscillating decay quickly as the particle current penetrate into the lead. The fast decay of the STT indicates the spin angular moment is almost absorbed near the interface. The lower insert of Fig. 2 gives the angular dependence of $T_{//}$ and $T_\perp$ calculated with scattering wave functions and $T_{//}$ by Eq. (1). The $T_{//}$ calculated by both methods are consistent well. So, in the following, we focus on the $T_{//}$ simply by Eq. (1). Moreover, our studies indicate that the ratio of $T_\perp/T_{//}$ is around 0.15, which is larger compared with that in the metallic spin-valve.

3 Electric STT in Fe/Vac/Fe MTJs

Electric STT in Fe/Vac/Fe should be a best system to test the electronic structure based STT calculation. Fig. 3 gives the $I_z^{(s)}$, $T_{//}$, and TMR with respect to the electric bias in Fe/Vac(5ML)/Fe with different surface roughness

$x = 0$, 0.05, 0.3, and 0.5. Here $x = 0$, 0.05, 0.3, and 0.5 correspond to zero, 5%, 30%, and 50% ad-atoms on the top of iron surfaces. For asymmetric MTJs, we calculated both negative and positive bias STT. $T_{//}$ and TMR show rich bias dependence with respect to the interface roughness.

For the MTJ with perfect interfaces, the results are shown in Fig. 3(a). $I_z^{(s)}(0)$ and $I_z^{(s)}(\pi)$ show odd and even symmetry, respectively. The former increases quickly at smaller bias and saturated at large bias with an inflection point around 0.5 V, the fast increasing at small bias relates to the minority-spin dominating transport in the PC.

There are surface states just above the Fermi level, a small bias will open the resonant channels and results in a fast increasing in transmission. Further increasing the bias will shift two surface states away from each other, so the resonant channel is very sensitive to the applied bias. $I_z^{(s)}(\pi)$ shows quadratic behavior, and get saturated at large bias. Consequently, the $T_{//}$ demonstrates a S shape with respect to bias. This is different comparing with perfect Fe/MgO/Fe, where $I_z^{(s)}(0)$ and $I_z^{(s)}(\pi)$ have linear and quadratic bias dependence when $V_b < 0.5$ V, respectively [5].

TMR decrease quickly from 300% at small bias state to almost 0% at 0.65 V, where the difference of the total current of the PC and APC is less than 0.5%, while the spin polarization of the PC and APC is 69 and −26%, respectively. TMR in Fe/Vac/Fe MTJs decrease more quickly than MgO-based MTJs as function of the applied bias [7], given another indication that minority-spin dominated system is more sensitive to applied bias than majority-spin dominated tunnelling process.

When the structure getting asymmetric, the behavior of the spin transport begin to deviate from the symmetry. Here, we study two roughness $x = 0.05$ [Fig. 3(b)] and 0.3 [Fig. 3(c)].The former is more close to the perfect sample both from point view of STT and TMR, while the later distort greatly from ideal, which can be considered as a transition state between the prefect one [Fig. 3(a)] to the heavily roughness one [Fig. 3(d)].

For $x = 0.3$, it completely loses the symmetry comparing with ideal situation. At the small bias, both $I_z^{(s)}(0)$ and $I_z^{(s)}(\pi)$ are linear with smaller negative gradient. At higher negative bias, $I_z^{(s)}(0)$ keeps linearly, while $I_z^{(s)}(\pi)$ gradually turns to a positive gradient. At higher positive bias, $I_z^{(s)}(0)$ gradually turns to a positive gradient with a sign change at 0.45 V, $I_z^{(s)}(\pi)$ turns to a larger negative gradient at the same time. Consequently, $T_{//}$ shows small value close to zero at small bias while decrease quickly at larger positive bias.

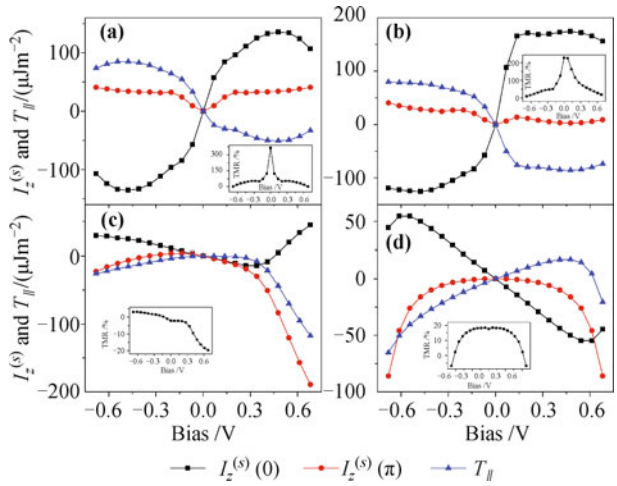

Fig. 3 Spin current $I_z^{(s)}$ and in-plane torque $T_{//}$ with magnetization angle $\theta = \pi/2$ in Fe/Vac(5ML)/Fe with interface roughness $x =$ **(a)** 0, **(b)** 0.05, **(c)** 0.3, and **(d)** 0.5.

The sign change at 0.45 V in $I_z^{(s)}(0)$ can be understood by the energy dependent transmission as shown in Fig. 4(a), where we find the majority-spin dominates the PC almost in all the energy windows at smaller bias of 0.34 V, while the minority-spin boosts up and begins to

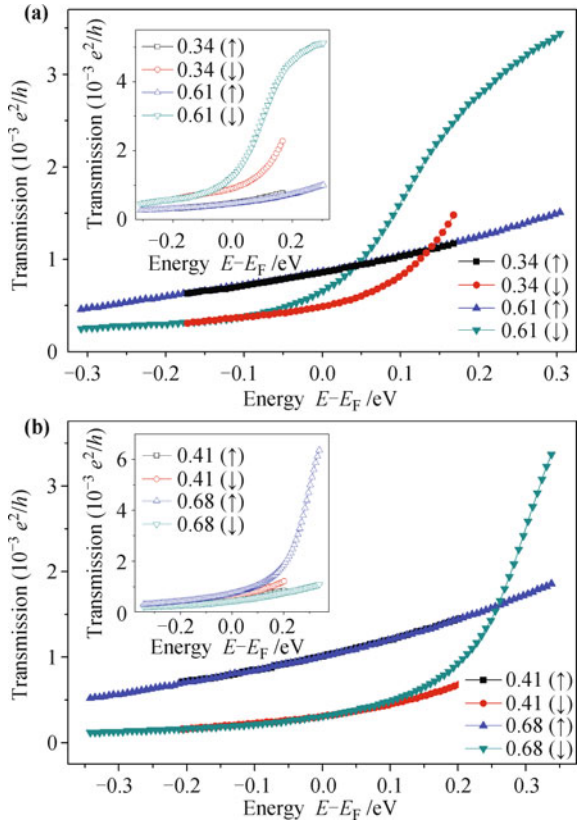

Fig. 4 Energy-dependent transmission of the PC and APC (insert) configurations of the Fe/Vac(5ML)/Fe with interface roughness **(a)** $x = 0.3$ and **(b)** $x = 0.5$ under bias voltage.

dominate the conductance around energy of 0.05 eV above Fermi level at higher bias of 0.61 V. Moreover, we notice negative TMR at equilibrium state and small negative and positive bias. This is consistent with the recent calculation, there a cross-over point is found around $x = 0.25$ [30].

When both the interfaces are extremely dirty with $x = 0.5$, the MTJ can be considered as a symmetric structure again. Here, $I_z^{(s)}(0)$ is linear with negative gradient in a large range of electronic bias, where the majority-spin dominates the conductance in full energy windows when $V_b < 0.5$ V as shown in Fig. 4(b). A rapid change around 0.55 V is related with the rapid increase of minority-spin conductance at higher bias as shown in Fig. 4(b). $I_z^{(s)}(\pi)$ keeps small values under the low bias, and the values suddenly increases at large bias. Consequently, $T_{//}$ keeps linear dependence on the applied voltage at small bias, but the curve changed at high positive bias and shows a sign change around 0.6 V. The behavior of $T_{//}$ is similar with MgO-based MTJs [5].

4 Thermo STT in Fe/Vac/Fe MTJs

Recently, both theoretical and experimental studies have demonstrated that temperature gradient can be used to generate STT more efficiently [6, 19–23]. Thermal conductance (or STT) depends on energy-dependent transmission (or spin-transmission) [6]. The resonant interfacial states dominate the transport in MTJs, which make the energy-dependent transmission (or spin-transmission) curvaceous. As a result, MTJs always show larger thermoelectric effects comparing with simple model prediction. The stronger the asymmetric of the transmission and spin-transmission around Fermi level, the larger the thermoelectric current and thermo-STT.

In Fig. 5 we give the energy-dependent transmission of the clean Fe/Vac/Fe MTJs with 5, 7, and 9 ML Vac barrier, and dirty 5 ML Vac barrier with $x = 0.5$. The minority-spin channels dominate the conductance for the clean MTJs, and the resonant peak around Fermi level gets sharper as barrier thickness increases. The heavily disordered interfaces make the majority-spin dominating in 5 ML $x = 0.5$. The slowly varied energy-dependent transmission around Fermi level make the Sommerfeld expansion valid to estimate thermoelectric current and thermo-STT, and small thermoelectric effect would be expected for the dirty MTJs.

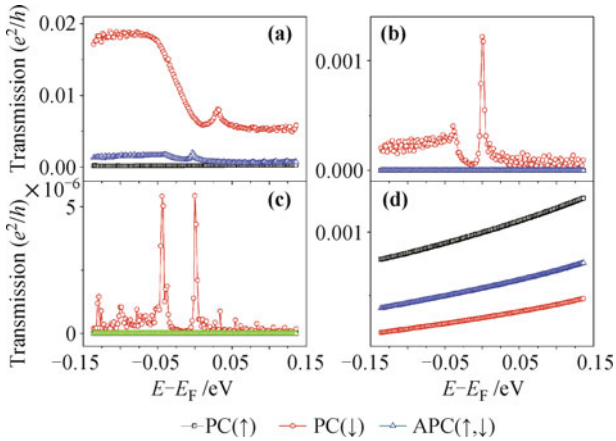

Fig. 5 Energy-dependent transmission of the PC and APC (insert) configurations of the Fe/Vac(nML)/Fe MTJs with $n = 5$ **(a)**, 7 **(b)**, 9 **(c)** with ideal interface, and **(d)** $n = 5$ with dirty interface $x = 0.5$.

Table 1 summarizes the thermoelectric effects and thermo-STT in clean Fe/Vac/Fe MTJs. Therein, Seebeck coefficient in all studied barriers shows same order for both PC and APC. Electric thermal conductance κ decreases more quickly than electric conductance. This is related to the sensitive dependence of the energy-dependent transmission [27, 34]. Consequently, ZT is surprisingly large in Fe/Vac/Fe MTJs in the absence of the phonon thermal conductance. The largest ZT of 6.2 is found in the 8 ML Vacuum barrier. The barrier thickness dependence of electronic torkance and thermo-STT show same trend as conductance, indicates that the spin

Table 1 Thermoelectric effects in nML Vac MTJs with clean interface at $T = 300$ K for PC/APC; thermo-STT at $T = 300$ K and $\Delta T = 1$ K for $\theta = 90°$. $T_{1K} = \tau_T \cdot 1$K and $\Delta V_{eq} = T_{1K}/\tau_V$ is the equivalent bias. S is Seebeck coefficient, $\kappa = \kappa_e$ is electric heat conductance. $ZT = GS^2T/\kappa$ is figure of merit.

n	G ($10^{12}\Omega^{-1}\cdot m^{-2}$)	S ($\mu V\cdot K^{-1}$)	κ ($MW\cdot K^{-1}\cdot m^{-2}$)	ZT	τ_V ($mJ\cdot V^{-1}\cdot m^{-2}$)	T_{1K}* ($nJ\cdot m^{-2}$)	ΔV_{eq} (μV)
4	22.2/10.6	33/48	117/40	0.06/0.19	–3.0	–125	42
5	3.3/1.4	58/43	31/2.9	0.1/0.27	–0.51	–45	89
6	0.90/0.16	52/37	3.9/0.14	0.19/0.48	–0.15	–6.5	44
7	0.58/6.2E-3	36/33	0.22/1.2E-6	1.2/0.38	–0.095	–0.61	6.4
8	0.11/4.1E-4	33/30	6.2E-3/2.3E-4	6.2/0.48	–0.019	–0.047	2.5
9	2.5E-3/1.0E-5	82/31	1.1E-3/9.5E-6	4.9/0.32	–4.2E-4	–0.012	29
10	1.0E-5/3.9E-7	12/29	1.2E-5/3.6E-7	3.3/0.28	–1.7E-5	–1.3E-3	76

*$1\,J\cdot V^{-1}\cdot m^{-2} = 3\times 10^{18}(\hbar/2)k\ \Omega^{-1}\cdot m^{-2}$

Table 2 Thermoelectric effects and thermo-STT in Fe/Vac(5ML)/Fe MTJs at $T = 300$ K for PC/APC configuration in the present of interface roughness.

n	G ($10^{12}\Omega^{-1}\cdot m^{-2}$)	S ($\mu V\cdot K^{-1}$)	κ ($MW\cdot K^{-1}\cdot m^{-2}$)	ZT	τ_V ($mJ\cdot V^{-1}\cdot m^{-2}$)	$T_{1K}{}^*$ ($nJ\cdot m^{-2}$)	ΔV_{eq} (μV)
0	3.3/1.4	58/43	31/2.9	0.1/0.27	–0.51	–45	89
0.05	3.5/1.2	39/21	25/4.2	0.062/0.037	–0.52	–30	58
0.3	0.65/0.66	–17/–18	2.2/2.2	0.026/0.032	0.023	–0.099	–4.3
0.5	0.63/0.53	–13/–14	2.5/1.7	0.013/0.020	0.052	–0.41	–7.9

polarization in all barriers keep same order. Thermo-STT in 4/6/8 ML Vac barrier show same order T_{1K} as that in Fe/MgO/Fe MTJs with 3/5/7 ML MgO barriers. ΔV_{eq} is the ratio of thermal torkance to electric torkance, which is large in thinner Vac barrier.

Effect of interface roughness on thermoelectric effects and thermo-STT in 5 ML Vac barrier is given in Table 2. Therein, Seebeck coefficient is positive in clean and slightly dirty MTJs, while change to negative in severely dirty samples. Electronic torkance change sign from negative in clean and slightly dirty sample to positive in severely dirty samples. Both the sign changes are related with the change of dominating spin channel as respect to the surface roughness. That is the minority-spin channel dominate in clean and slightly dirty situations, while change to majority-spin in heavily dirty situation. ZT decrease as interface roughness increase. Thermo-STT in dirty situation is considerable smaller than clean situation.

5 Summary

We present first-principle calculations of the electric and thermo STT in Fe/Vac/Fe MTJs in the presence of interface roughness. Our studies demonstrate rich bias dependence of $I_z^{(s)}$, $T_{//}$ and TMR behaviors with respect to the interface roughness. We observe an unusual non-monotonic bias dependence of $T_{//}$ in the heavily rough interface, where a sign reversal occur around 0.6 V. Thermoelectric effects in Fe/Vac/Fe MTJs is remarkable. We observe larger ZT of 6.2 in 8 ML clean Vacuum barrier, where the laking of phonon thermal conductance should be responsible for it. Thermo-STT in Fe/Vac/Fe MTJs show same order as that in Fe/MgO/Fe MTJs with similar barrier thickness. The large thermoelectric effects indicate that the signal build by thermal bias may be found application in scanning tunnelling microscope.

Acknowledgements We gratefully acknowledge financial support from the National Basic Research Program of China (973 Program) under the grant Nos. 2011CB921803 and 2012CB921304 and the National Natural Science Foundation of China grant Nos. 11174037 and 11274094.

References

1. H. Kubota, A. Fukushima, K. Yakushiji, T. Nagahama, S. Yuasa, K. Ando, H. Maehara, Y. Nagamine, K. Tsunekawa, D. D. Djayaprawira, N. Watanabe, and Y. Suzuki, Quantitative measurement of voltage dependence of spin-transfer torque in MgO-based magnetic tunnel junctions, *Nat. Phys.*, 2008, 4(1): 37
2. J. C. Sankey, Y. T. Cui, J. Z. Sun, J. C. Slonczewski, R. A. Buhrman, and D. C. Ralph, Measurement of the spin-transfer-torque vector in magnetic tunnel junctions, *Nat. Phys.*, 2008, 4(1): 67
3. A. M. Deac, A. Fukushima, H. Kubota, H. Maehara, Y. Suzuki, S. Yuasa, Y. Nagamine, K. Tsunekawa, D. D. Djayaprawira, and N. Watanabe, Bias-driven high-power microwave emission from MgO-based tunnel magnetoresistance devices, *Nat. Phys.*, 2008, 4(10): 803
4. D. C. Ralph and M. D. Stiles, Spin transfer torques, *J. Magn. Magn. Mater.*, 2008, 320(7): 1190
5. X. Jia, K. Xia, Y. Ke, and H. Guo, Nonlinear bias dependence of spin-transfer torque from atomic first principles, *Phys. Rev. B*, 2011, 84(1): 014401
6. X. Jia, K. Xia, and G. E. W. Bauer, Thermal spin transfer in Fe/MgO/Fe tunnel junctions, *Phys. Rev. Lett.*, 2011, 107(17): 176603
7. Y. Ke, K. Xia, and H. Guo, Oxygen-vacancy-induced diffusive scattering in Fe/MgO/Fe magnetic tunnel junctions, *Phys. Rev. Lett.*, 2010, 105(23): 236801
8. C. Wang, Y. T. Cui, J. A. Katine, R. A. Buhrman, and D. C. Ralph, Time-resolved measurement of spin-transfer-driven ferromagnetic resonance and spin torque in magnetic tunnel junctions, *Nat. Phys.*, 2011, 7(6): 496
9. S. Yuasa, T. Nagahama, A. Fukushima, Y. Suzuki, and K. Ando, Giant room-temperature magnetoresistance in single-crystal Fe/MgO/Fe magnetic tunnel junctions, *Nat. Mater.*, 2004, 3(12): 868
10. J. C. Slonczewski, Current-driven excitation of magnetic multilayers, *J. Magn. Magn. Mater.*, 1996, 159: L1
11. L. Berger, Emission of spin waves by a magnetic multilayer traversed by a current, *Phys. Rev. B*, 1996, 54: 9353
12. I. Theodonis, N. Kioussis, A. Kalitsov, M. Chshiev, and W. H. Butler, Anomalous bias dependence of spin torque in magnetic tunnel junctions, *Phys. Rev. Lett.*, 2006, 97(23): 237205

13. J. C. Slonczewski, Currents, torques, and polarization factors in magnetic tunnel junctions, *Phys. Rev. B*, 2005, 71(2): 024411
14. J. Xiao, G. Bauer, and A. Brataas, Spin-transfer torque in magnetic tunnel junctions: Scattering theory, *Phys. Rev. B*, 2008, 77(22): 224419
15. M. Wilczyński, J. Barnaś, and R. Świrkowicz, Free-electron model of current-induced spin-transfer torque in magnetic tunnel junctions, *Phys. Rev. B*, 2008, 77(5): 054434
16. A. Manchon, N. Ryzhanova, A. Vedyayev, M. Chschiev, and B. Dieny, Description of current-driven torques in magnetic tunnel junctions, *J. Phys.: Condens. Matter*, 2008, 20(14): 145208
17. S. Wang, Y. Xu, and K. Xia, First-principles study of spin-transfer torques in layered systems with noncollinear magnetization, *Phys. Rev. B*, 2008, 77(18): 184430
18. Z. Yuan, S. Wang, and K. Xia, Thermal spin-transfer torques on magnetic domain walls, *Solid State Commun.*, 2010, 150(11–12): 548
19. C. Heiliger and M. D. Stiles, Ab initio studies of the spin-transfer torque in magnetic tunnel junctions, *Phys. Rev. Lett.*, 2008, 100(18): 186805
20. G. E. W. Bauer, A. H. MacDonald, and S. Maekawa, Spin caloritronics, *Solid State Commun.*, 2010, 150(11–12): 459
21. G. E. W. Bauer, E. Saitoh, and B. J. van Wees, Spin caloritronics, *Nat. Mater.*, 2012, 11(5): 391
22. M. Hatami, G. E. W. Bauer, Q. F. Zhang, and P. J. Kelly, Thermal spin-transfer torque in magnetoelectronic devices, *Phys. Rev. Lett.*, 2007, 99(6): 066603
23. M. Hatami, G. E. W. Bauer, Q. Zhang, and P. J. Kelly, Thermoelectric effects in magnetic nanostructures, *Phys. Rev. B*, 2009, 79(17): 174426
24. H. Yu, S. Granville, D. P. Yu, and J. Ph. Ansermet, Evidence for thermal spin-transfer torque, *Phys. Rev. Lett.*, 2010, 104(14): 146601
25. J. C. Slonczewski, Initiation of spin-transfer torque by thermal transport from magnons, *Phys. Rev. B*, 2010, 82(5): 054403
26. G. Autès, J. Mathon, and A. Umerski, Theory of tunneling magnetoresistance of Fe/GaAs/Fe(001) junctions, *Phys. Rev. B*, 2010, 82: 115212
27. X. Jia and K. Xia, Thermal electric effects in Fe-GaAs-Fe tunnel junctions, *AIP Advances*, 2012, 2(4): 041411
28. P. Vlaic, N. Baadji, M. Alouani, H. Dreysse, O. Eriksson, O. Bengone, and I. Turek, Calculated electronic and transport properties of Fe/GaAs/Fe(001) tunnel junctions, *Surf. Sci.*, 2004, 566–568: 303
29. V. Popescu, H. Ebert, N. Papanikolaou, R. Zeller, and P. H. Dederichs, Influence of spin-orbit coupling on the transport properties of magnetic tunnel junctions, *Phys. Rev. B*, 2005, 72(18): 184427
30. P. X. Xu, V. M. Karpan, K. Xia, M. Zwierzycki, I. Marushchenko, and P. J. Kelly, Influence of roughness and disorder on tunneling magnetoresistance, *Phys. Rev. B*, 2006, 73: 180402(R)
31. Y. Ke, K. Xia, and H. Guo, Disorder scattering in magnetic tunnel junctions: Theory of nonequilibrium vertex correction, *Phys. Rev. Lett.*, 2008, 100(16): 166805
32. I. Turek, V. Drchal, J. Kudrnovský, M. Šob, and P. Weinberger, Electronic Structure of roughnessed Alloys, Surfaces and Interfaces, Boston: Kluwer, 1997
33. S. H. Vosko, L. Wilk, and M. Nusair, Accurate spin-dependent electron liquid correlation energies for local spin density calculations: A critical analysis, *Can. J. Phys.*, 1980, 58(8): 1200
34. H. van Houten, L. W. Molenkamp, C. W. J. Beenakker, and C. T. Foxon, Thermo-electric properties of quantum point contacts, *Semicond. Sci. Technol.*, 1992, 7(3B): B215